CrystEngComm

Cite this: *CrystEngComm*, 2012, **14**, 8440–8445

www.rsc.org/crystengcomm

**PAPER**



# Facile synthesis, optical properties and growth mechanism of elongated Mn-doped $ZnSe_{1-x}S_x$ nanocrystals

**Tingting Yao,[a] Shufang Kou,[b] Yanghui Sun,[c] Qing Zhao[c] and Jian Yang*[ab]**

***Received 19th August 2012, Accepted 23rd September 2012***
**DOI: 10.1039/c2ce26322j**

Transition-metal doping in semiconductors is an important way to modulate their intrinsic properties or bring out new functionalities for applications. Here, elongated Mn-doped $ZnSe_{1-x}S_x$ nanocrystals are synthesized through a facile one-pot reaction under mild conditions. These $ZnSe_{1-x}S_x$ nanocrystals with a diameter of 2–4 nm have a cubic phase structure. EPR and PL spectra confirm the successful doping of $Mn^{2+}$ into the $ZnSe_{1-x}S_x$ nanocrystals, based on the corresponding hyperfine splitting constants and emission bands. The temporal evolution of UV-vis absorption and PL spectra indicates the growth-doping mechanism for the formation of the doped nanocrystals. Surface coating of these nanocrystals with a shell increases the quantum yield up to 35%. And the dual-function role of 1-dodecanethiol is confirmed in the formation of the elongated Mn-doped $ZnSe_{1-x}S_x$ nanocrystals.

## Introduction

Mn-doped ZnE (E = Se or S) nanocrystals have attracted extensive attention in the past decade, due to their strong and stable emission from the $^4T_1 \rightarrow {}^6A_1$ transition of $Mn^{2+}$ in the host lattice and large Zeeman splitting from the sp–d exchange interaction between transition metal ions and host semiconductor.[1] The high quantum yield and good stability of the emission, plus the low toxicity of Mn-doped ZnE nanocrystals in cells, make the doped nanocrystals a promising optical label for biological imaging.[2] The large Stokes shift of the emission effectively reduces its self-quenching, enabling the doped nanocrystals to be used in optoelectronics, such as LEDs, solar cells, *etc*.[3,4] In addition, the doped nanocrystals are also reported as an electrocatalyst for the oxidation of ethanol.[5]

Mn-doped $ZnSe_{1-x}S_x$ nanocrystals are more attractive but less studied in comparison with Mn-doped ZnSe or ZnS, although they present a tunable band-gap for the desired semiconductor engineering. The traditional synthesis strategy involved with organometallic salts ($MnMe_2$ and $ZnMe_2$) does not work well for such doped nanocrystals, because the band-gap emission is easily observed besides the dopant-related emission.[6,7] Using metal oxide nanocrystals as the dopant source, instead of the organometallic salts, successfully produced the highly emissive nanocrystals though the growth-doping strategy.[8] Recently, Zeng *et al.* synthesized the Mn-doped ZnSeS nanocrystals through the epitaxial growth of ZnS on Mn-doped ZnSe nanocrystals, followed with a high-temperature annealing of the core–shell nanocrystals.[9] Unfortunately, these syntheses need the preparation and purification of another nanocrystal like metal oxide or Mn-doped ZnSe nanocrystals in advance. The multiple reaction steps might cause severe issues, such as time-consuming, low reproducibility, and inevitable loss of the product.

The shape control of Mn-doped $ZnSe_{1-x}S_x$ nanocrystals has not been realized, because the doping of transition metal ions into anisotropic nanocrystals is much more difficult than that for spherical ones.[1] Even for Mn-doped ZnSe or ZnS nanowires/nanorods, only a few studies have been reported.[10–14] Park *et al.* made use of gold nanoparticles on a silicon substrate as a catalyst to induce the formation of Mn-doped ZnSe nanowires *via* chemical vapor deposition at 800 °C.[10] The high temperature reaction was also employed for Mn-doped ZnSe nanowires coated with carbon.[11] The Mn-doped ZnSe nanowires could be fabricated by $Li_4[Zn_{10}Se_4(SPh)_{16}]$ and $MnSt_2$ in hexadecylamine at a low temperature,[12] or by $[Zn_{1-x}Mn_xSe](DETA)_{0.5}$ nanobelts as a template.[13] Liu and coworkers injected the oleylamine-S solution into the mixture of $Zn(NO_3)_2$, $Mn(NO_3)_2$, 1-dodecanethiol and oleylamine at 160 °C. After annealing at 230 °C, the solution gave a large quantity of Mn-doped ZnS quantum rods.[14]

Herein, the one-pot synthesis of elongated Mn-doped $ZnSe_{1-x}S_x$ nanocrystals, denoted as ED-NCs, is achieved under mild experimental conditions. This synthesis does not necessitate a complicated preparation before the synthesis. The as-prepared ED-NCs are characterized by XRD, TEM, EPR, UV-vis absorption spectra and PL spectra, all of which confirm the successful doping of Mn into the nanocrystals. The doping mechanism has been revealed by control experiments and *ex situ* monitoring with UV-vis absorption spectra and PL spectra. Finally, the roles of the surfactants in the reaction are discussed in detail.

[a]*Department of Chemical Engineering, South China University of Technology, Guangzhou, P. R. China. E-mail: yangjian@scut.edu.cn*
[b]*Department of Chemistry, Shandong University, Jinan, P. R. China. Fax: +86-531-88364489; Tel: +86-531-88364489*
[c]*State Key Laboratory for Mesoscopic Physics and Department of Physics, Electron Microscopy Laboratory, Peking University, Beijing, P. R. China*

## Experimental

### Materials

Methanol (99.5%) and hexane (99.5%) were obtained from Sinopharm Chemical Reagent Co. Ltd. Selenium powder (Se, 99.5%), oleylamine (OAm, 80–90%), 1-dodecanethiol (DDT, 98%), and anhydrous manganese(II) chloride ($MnCl_2$, 97%) were ordered from ACROS organics. Zinc acetate dihydrate ($ZnAc_2{\cdot}2H_2O$, 99%) was purchased from Guangzhou Chemical Reagent Factory. Tri-butyl phosphine (TBP, 95%) was obtained from Aladdin Chemical Reagent Co. Ltd. Selenium dioxide ($SeO_2$, 98%) was ordered from Guanghua Chemistry Factory Co. Ltd. in Guangzhou. All these reagents were used without any further purification.

### Synthesis of Mn-doped $ZnSe_{1-x}S_x$ nanocrystals

In a typical procedure, 0.15 mmol of $ZnAc_2{\cdot}2H_2O$, 0.0225 mmol of $MnCl_2$, 0.125 mL of DDT and 3 mL of OAm were loaded in a three-neck flask. The flask was sealed with a rubber stopper and a thermocouple, vacuumed by a Schlenk line, and flushed with nitrogen to remove oxygen and moisture in the flask. Separately, the TBPSe stock solution was prepared by dissolving 0.3 mmol Se in 0.1 mL of TBP and 0.7 mL of OAm inside the glove box. The TBPSe stock solution was injected into the flask at room temperature. The obtained solution was heated to 200 °C as quickly as possible under nitrogen atmosphere and kept at that temperature for ten minutes. Then, the solution was further heated to 260 °C, and maintained for another 10–15 minutes to grow the Mn-doped $ZnSe_{1-x}S_x$ nanocrystals.

### Shell growth

A $ZnSe_{1-x}S_x$ shell was grown on the surface of the Mn-doped $ZnSe_{1-x}S_x$ nanocrystals by a SILAR procedure. When the desired size of the Mn-doped $ZnSe_{1-x}S_x$ nanocrystals was reached, the temperature was reduced to 240 °C. 0.207 mL of 0.1 M $ZnAc_2{\cdot}2H_2O$ in OAm was injected slowly into the solution and a strong emission enhancement could be immediately observed. The same volume of 0.1 M $SeO_2$ in OAm was then added into the solution to react with the Zn precursor. Meanwhile, DDT in the solution continuously decomposed, resulting in the growth of a $ZnSe_{1-x}S_x$ shell. After the solution was cooled to room temperature, the product was precipitated by addition of methanol and collected by centrifugation. The as-obtained white powders could be well dispersed in many non-polar solvents, such as hexane, chloroform, toluene, *etc.*

### Characterization

X-ray diffraction (XRD) patterns were obtained on an X-ray diffractometer (D8 Advance, Germany) equipped with a rotating anode, using monochromatic Cu Kα as the radiation source. The working voltage and current of the diffractometer were kept at 40 kV and 40 mA, respectively. Transmission electron microscopy (TEM) images were acquired with a JEM-1011 transmission electron microscope at an accelerating voltage of 100 kV. High-resolution TEM (HRTEM) images were obtained with a JEOL 2010 analytic transmission electron microscope working at 200 kV. Energy dispersion X-ray spectroscopy (EDS) spectra were recorded on a scanning electron microscope (JEOL JSM-7600F) equipped with an energy dispersion X-ray spectrometer (Oxford INCA sight X). The samples for TEM images and EDS spectra were purified by centrifugation, in order to remove the surfactants and/or the excess of the reactants. Then, the nanocrystals were dispersed in hexane. Several aliquots of the solution were dropped on a copper grid coated with an ultrathin amorphous carbon film and the grids were dried at room temperature. The electron paramagnetic resonance (EPR) spectra were recorded on an electron paramagnetic resonance spectrometer (JEOL JES-FA200), using the microwave of 9.45 GHz. UV-vis absorption spectra were recorded in the range of 250–700 nm at room temperature by a Shimadzu UV-2450 spectrophotometer. Photoluminescence (PL) spectra were obtained from a Thermo lumina fluorometer (Thermo lumina 222-263000) at room temperature.

## Results and discussion

### Structure and composition

The typical X-ray diffraction pattern of the obtained product is presented in Fig. 1a. The diffraction peaks at 27.88°, 46.31° and 54.18° can be attributed to the (111), (220) and (311) planes of cubic-phase $ZnSe_{1-x}S_x$ respectively. The lattice constant calculated from these peaks is 5.563 Å, giving a content of sulfur ($x$) of about 40% based on Vegard's law.[15] The low intensity and broad width of the diffraction peaks indicate the poor crystallinity and small size of $ZnSe_{1-x}S_x$, both of which are directly confirmed by TEM microscopy. A similar phenomenon is also observed in the diffraction pattern of the core–shell NCs, as shown in Fig. 2a. The calculated lattice constant of the core–shell NCs ($a$ = 5.589 Å) is a little larger than that of the core, implying higher content of selenium in the core–shell NCs. The result could be attributed to the introduction of an additional Se stock solution into the reaction for the growth of the shell.

The shape and size of the products were investigated by TEM microscopy. Fig. 1b shows a typical TEM image of the product, in which rod-like and branched nanocrystals could be easily

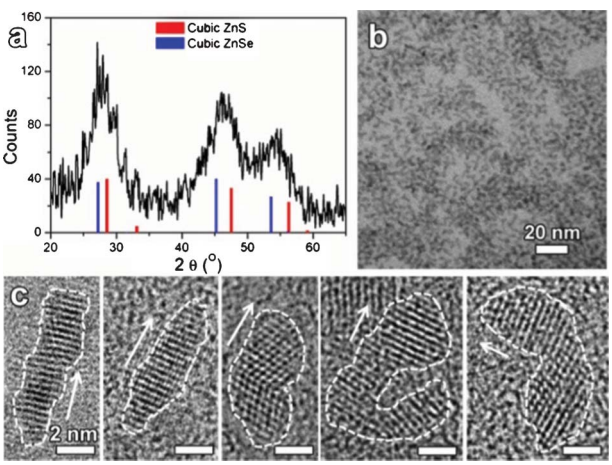


**Fig. 1** XRD pattern (a), TEM (b), and HRTEM images (c) of the elongated Mn-doped $ZnSe_{1-x}S_x$ nanocrystals. The arrows indicate the [111] direction and all the scale bars are 2 nm.

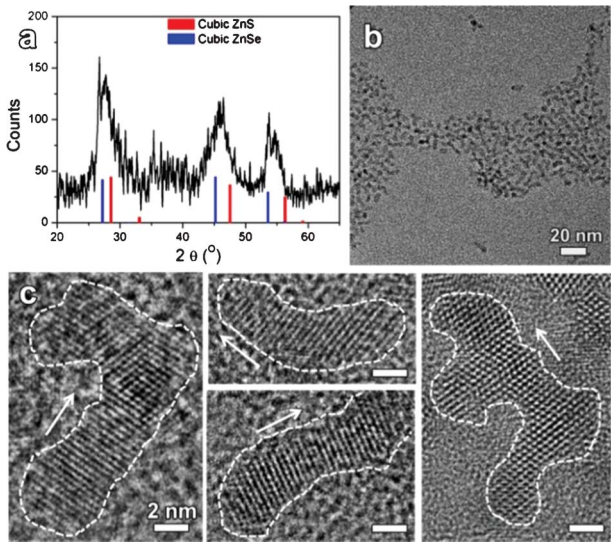


**Fig. 2** XRD pattern (a), TEM (b), and HRTEM images (c) of the elongated core–shell nanocrystals. The arrows indicate the [111] direction and all the scale bars are 2 nm.

observed. To the best of our knowledge, such a one-dimensional nanostructure is seldom reported for doped nanocrystals.[12,13,16,17]

The elongated nanocrystals exhibit a relatively narrow size distribution in terms of diameter, but their lengths vary widely from 4 nm to 10 nm. HRTEM images of the elongated nanocrystals show the clear lattice fringes that correspond to the crystal planes of (111). Associated with the nanocrystal shape, it can be concluded that the elongated nanocrystals grow along the [111] direction. Meanwhile, a lot of structural defects like stacking faults, fringe bending, *etc.*, are also presented in the HRTEM images. The surface ligands on the quantum dots, or the incomplete match between the neighboring quantum dots in crystallographic orientation would lead to the formation of these defects.[18,19] In fact, the oriented-attachment growth has been reported for many nanorods synthesized in alkyl amines.[20–24] The same morphology is also observed for the core–shell NCs (Fig. 2b, 2c).

Because of the reduced dopant amount and the high compatibility of MnSe with cubic ZnE (E = Se or S) lattice,[25] it is hard to identify the existence of Mn in the elongated nanocrystals merely by TEM and XRD. So, EPR spectra are used to verify the presence of Mn, because it strongly depends on unpaired electrons in materials. As presented in Fig. 3, the EPR spectrum of the elongated nanocrystals shows a well-resolved six-line pattern that could be attributed to the hyperfine interaction of unpaired electrons with the $^{55}$Mn nuclear spin ($I$ = 5/2).[26] The hyperfine constant of 68.5 G obtained from this pattern further confirms that $Mn^{2+}$ ions in the host nanocrystals likely substitute $Zn^{2+}$ at the tetrahedral sites, or insert into the cubic zinc-blende lattice at the interstitial sites.[8,27] Otherwise, a hyperfine splitting constant about 95 G would be expected for $Mn^{2+}$ ions on the particle surface.[28] The aggregation or clustering of $Mn^{2+}$ ions in the elongated nanocrystals could be excluded, due to the good resolution of hyperfine splitting.[11,29] As for the core–shell nanocrystals, the same six-line pattern is observed in the EPR spectrum, indicating that $Mn^{2+}$ ions are still

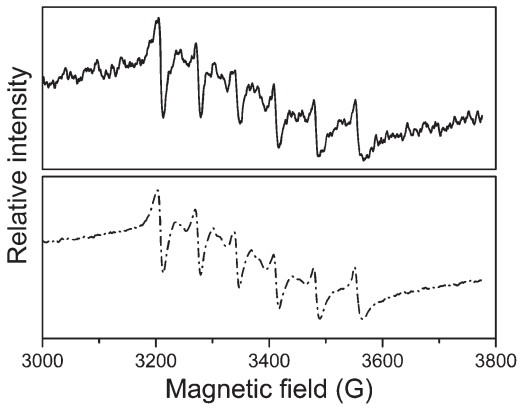


**Fig. 3** EPR spectra of the elongated Mn-doped $ZnSe_{1-x}S_x$ nanocrystals (solid line) and their core–shell nanocrystals (dash dot line).

maintained. The high temperature growth of the shell does not result in the diffusion of $Mn^{2+}$ out from the nanocrystals.

Fig. 4 shows the typical UV-vis absorption spectra and PL spectra of the elongated Mn-doped $ZnSe_{1-x}S_x$ nanocrystals (ED-NCs) and their core–shell nanocrystals. The UV-vis absorption spectrum of the ED-NCs shows an absorption shoulder with its onset at 384 nm, which gives information about the size and band gap of the host material ($ZnSe_{1-x}S_x$). Compared with the undoped samples, there is no remarkable change for the ED-NCs in terms of UV-vis absorption spectrum. But the case of PL spectra is totally different. The substitution of $Zn^{2+}$ with $Mn^{2+}$ in $ZnSe_{1-x}S_x$ would make the degeneracies of the electronic structure decrease and generate localized levels of $^4T_1$ and $^6A_1$ within the band gap of $ZnSe_{1-x}S_x$ nanocrystals.[7] So, when the $ZnSe_{1-x}S_x$ nanocrystals are irradiated by the excitation light, the energy transfer from the host material to the dopant occurs immediately, resulting in an intense emission around 570–580 nm.[25] This strong emission from $^4T_1 \rightarrow {}^6A_1$ transition of $Mn^{2+}$ in $ZnSe_{1-x}S_x$ at 575 nm is observed in Fig. 4 as expected, suggesting the successful doping of $Mn^{2+}$ into $ZnSe_{1-x}S_x$. Meanwhile, the emission from the band edge of the host material is completely inhibited, indicating the high efficiency of the energy transfer between the host material and the dopant.

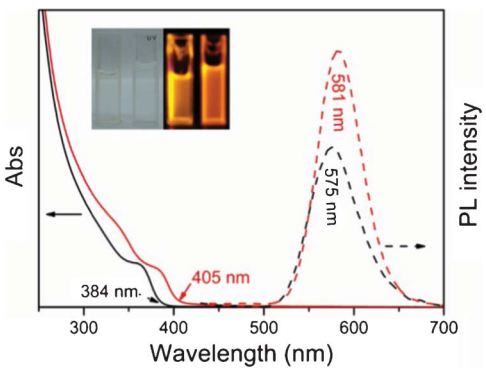


**Fig. 4** UV-vis absorption spectra (solid line) and PL spectra (dash line) of the elongated Mn-doped $ZnSe_{1-x}S_x$ nanocrystals (black line) and their core–shell nanocrystals (red line). Inset figure shows the digital images of these products obtained with or without the irradiation of a hand-held lamp (left, the doped nanocrystals; right, their core–shell nanocrystals).

 

The quantum yield of the emission at 575 nm is approximately 20%, lower than that from the spherical ones.[9] It can be attributed to the emission quenching due to structural defects inside the ED-NCs. Accompanying with the shell growth, the absorption onset shows a significant red-shift to 405 nm, indicating the size increasing of nanocrystals and the successful coating of the shell. At the same time, the emission from the $^4T_1 \rightarrow {}^6A_1$ transition of $Mn^{2+}$ in $ZnSe_{1-x}S_x$ moves to 581 nm, suggesting the well maintenance of $Mn^{2+}$ inside the core–shell nanocrystals. The quantum yield of the core–shell nanocrystals is improved to approximately 35%, due to the effective surface passivation. The inset image of Fig. 4 shows the digital real-color images of the ED-NCs and their core–shell nanocrystals with or without the irradiation of a hand-held lamp. Both of them display intense orange emissions.

## Growth mechanism

Fig. 5 shows the temporal evolution of the UV-vis absorption spectra and PL spectra of the solution during the synthesis of the ED-NCs. As the reaction proceeds at 200 °C for 5 minutes, there is no obvious absorption band in the UV-vis absorption spectra. The PL spectrum of the same solution shows a broad emission band around 420 nm that might be assigned to the radiative recombination related with the surface and/or structural defects in $ZnSe_{1-x}S_x$ clusters.[14,30] The absence of the emission around 560–580 nm indicates that $Mn^{2+}$ ions neither adsorb on the surface of clusters nor enter into the clusters. Thus, the solution is heated from 200 °C to 260 °C to activate the precursor of $Mn^{2+}$ and promote its doping, because the decomposition of the Mn precursor usually needs a higher reaction temperature than that for the Zn precursor.[25] It is found that the typical absorption feature of the $ZnSe_{1-x}S_x$ nanocrystals appears in the absorption spectra at 247 °C, although the emission caused by the dopant of $Mn^{2+}$ is still absent from the PL spectrum. This result indicates the formation of $ZnSe_{1-x}S_x$ nanocrystals is ahead of the doping of $Mn^{2+}$. On the other hand, the presence of $ZnSe_{1-x}S_x$ nanocrystals also allows them to act as a seed to adsorb $Mn^{2+}$ and facilitate the doping process. When the reaction temperature reaches 258 °C, the absorption peak of $ZnSe_{1-x}S_x$ nanocrystals displays an obvious red-shift in comparison with that observed at 247 °C, suggesting the growth of the nanocrystals. Most importantly, the emission related with $Mn^{2+}$ is observed in the PL spectrum, indicating the successful incorporation of $Mn^{2+}$ into the host material. The low intensity of this emission might be attributed to low concentration of $Mn^{2+}$ per $ZnSe_{1-x}S_x$ nanocrystal or nonradiative recombination pathways.[31] Annealing the nanocrystals in the solution at 260 °C for 4 minutes makes the emission intensity significantly increased, implying the increased number of $Mn^{2+}$ inside $ZnSe_{1-x}S_x$ nanocrystals. Meanwhile, the annealing of the nanocrystals would also benefit the elimination of the surface and structural defects, resulting in the disappearance of the emission band centered about 420 nm from the PL spectrum. Based on the above facts, the ED-NCs are more likely to be formed through a growth-doping mechanism, rather than a nucleation-doping mechanism.

The control experiments are conducted to further support the growth-doping mechanism for the formation of the ED-NCs. In order to slow down the nucleation and growth of the ED-NCs for a clear scenario about the underlying mechanism, the reaction is kept at low temperature (200 °C) for 30 minutes during the whole process. If zinc acetate is used as the only metal precursor for the reaction, the obtained solution shows an absorption shoulder at 320 nm (Fig. 6a, inset), indicating the formation of semiconductor nanocrystals. The PL spectrum shows a strong emission at 350 nm from the band-gap edge and a

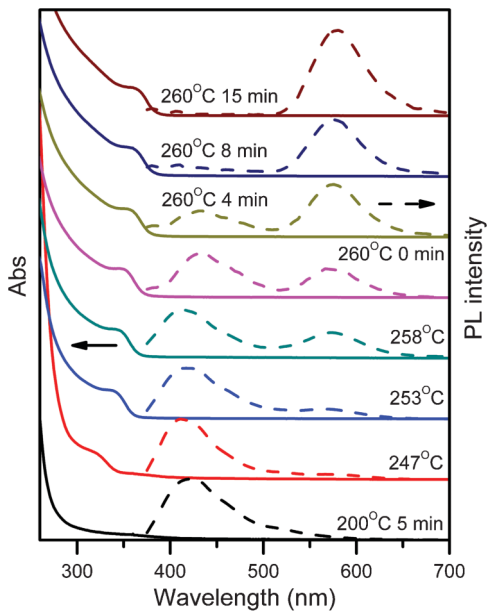


**Fig. 5** UV-vis absorption (solid line) and PL spectra (dash line) of the product obtained at different reaction times during the growth of the elongated Mn-doped $ZnSe_{1-x}S_x$ nanocrystals.

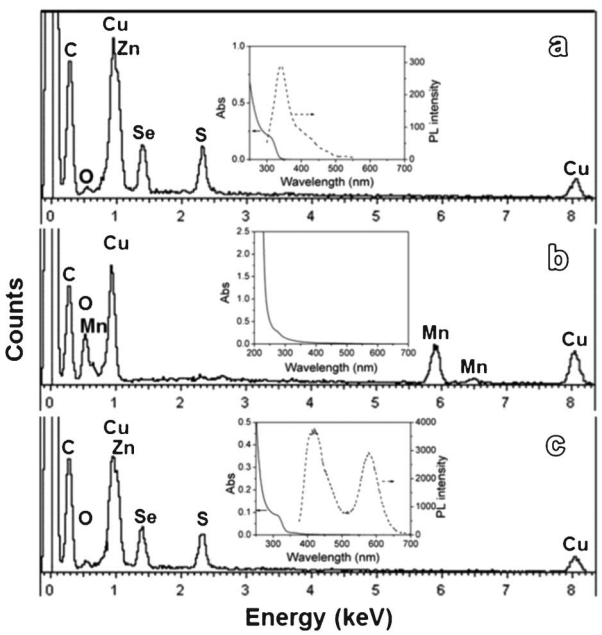


**Fig. 6** EDS spectra of the products obtained by using different metal precursors in the reaction at 200 °C for 30 min. (a) $ZnAc_2{\cdot}2H_2O$, (b) $MnCl_2$, (c) $ZnAc_2{\cdot}2H_2O$ and $MnCl_2$. The inset figures show the corresponding UV-vis absorption spectra (solid line) and PL spectra (dash line).

weak shoulder at 420 nm from surface defects or structural defects. It is believed that the absence of $Mn^{2+}$ in the solution effectively avoids the interferences from the impurities to the nucleation and growth process, reduces the defect density inside the nanocrystals, and then leads to a stronger band-edge emission than that observed in the presence of the $Mn^{2+}$ precursor. The EDS spectrum reveals the signals of Zn, Se, and S, implying the successful formation of the $ZnSe_{1-x}S_x$ nanocrystals under these experimental conditions. When manganese dichloride is used as the only metal precursor for the reaction, no obvious peaks could be observed in the absorption spectrum and the PL spectrum, as shown in Fig. 6b. Furthermore, the signals of Se and S do not appear in the EDS spectrum of the product. This result indicates that MnE (E = S, Se) is hard to be formed under the same experimental conditions. When both zinc acetate and manganese dichloride are added into the solution, the absorption peak of $ZnSe_{1-x}S_x$ appears in the absorption spectrum again (Fig. 6c). Meanwhile, the emission band at 420 nm due to the presence of surface defects or structural defects and the emission band at 580 nm caused by the incorporation of $Mn^{2+}$ could also be clearly observed. Because of the low doping content, there is no signal of Mn in the EDS spectrum. The results indicate that the formation of $ZnSe_{1-x}S_x$ nanocrystals is much easier than that of MnSe in our case, consistent with the growth-doping mechanism.

The formation process of the ED-NCs *via* the growth-doping mechanism could be described in Scheme 1. At the beginning of the reaction, the Zn precursor starts to decompose and generate a large number of clusters. These clusters would gradually grow in size and then generate the quantum dots of $ZnSe_{1-x}S_x$, resulting in the typical absorption feature of semiconductor nanocrystals. Since there are a large number of surface defects and structural defects on the quantum dots, the emission related with these defects dominate the PL spectrum. The huge surface area of these quantum dots provides a myriad of sites for the Mn species to adsorb on the surface *via* the interaction between S/Se and Mn. Meanwhile, the presence of the quantum dots would facilitate the decomposition of the Mn species at high temperature, due to the low energy barrier in nucleation on the existing surface. So, the emission bands caused by $Mn^{2+}$ could be clearly observed in the PL spectrum, although the intensity is still quite weak. At the same time, $ZnSe_{1-x}S_x$ would also continuously overgrow to coat $Mn^{2+}$ ions and make them incorporated. As the reaction keeps going, the number of $Mn^{2+}$ incorporated into $ZnSe_{1-x}S_x$ would remarkably increase, resulting in a highly luminescent emission band from $Mn^{2+}$. The surface defects and structural defects are gradually eliminated from the host material by annealing at a high reaction temperature. So, the defect-related emission disappears from the PL spectrum. During this process, these quantum dots would self-assemble together to become elongated nanocrystals *via* oriented-attachment mechanism.

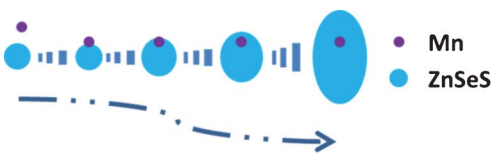


**Scheme 1** The schematic formation process of the elongated Mn : $ZnSe_{1-x}S_x$ nanocrystals.

Fig. 7a shows the influence of the manganese precursor on the optical properties of the products. The absorption onset presents a slight change, as the molar ratio of Mn/Zn varies from 5–15%. But the increasing of Mn would lead to more $Mn^{2+}$ ions adsorbed on the particle surface and then incorporated into the host lattice. As a result, the emission related with the dopant gives a red-shift from 575 nm to 580 nm, and an enhanced quantum yield due to the increasing number of $Mn^{2+}$ in the ED-NCs. However, the continuous increasing of the Mn precursor would result in strong Mn–Mn interactions, as shown in Fig. 7b. The resolved emission centered at 650 nm originates from the Mn–Mn centers, similar to the result reported by Pradhan and Peng.[32]

Finally, it should be noted that the type and quantity of the surfactants are important to the formation of ED-NC nanocrystals. In our case, there are two surfactants in the reaction, oleylamine and 1-dodecanethiol. The former as an activator for the decomposition of metal carboxylates, has been applied in the preparation of many high-quality quantum dots.[33] Both manganese oxide and zinc oxide nanoparticles could be obtained by thermal decomposition of metal carboxylates using oleylamine as the solvent at 150–240 °C.[8,34] In order to avoid the formation of these oxides, 1-dodecanethiol is introduced into the reaction to coordinate with the metal ions, which is supported by the obvious spectra change before and after the addition of 1-dodecanethiol in Fig. 8. On the other hand, 1-dodecanethiol would also act as a sulfur source for the formation of $ZnSe_{1-x}S_x$ at a high temperature. It is believed that the dual functions of

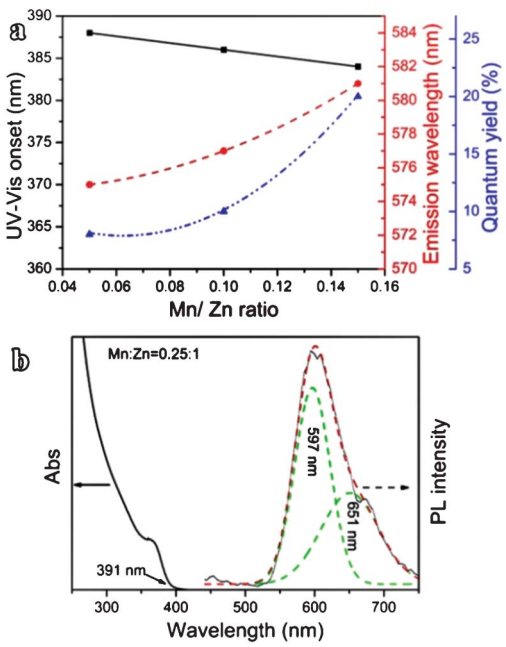


**Fig. 7** (a) The relationship of UV-vis onset (black), emission band (red) and quantum yield (blue) of the products with different molar ratios of Mn/Zn. (b) UV-vis absorption spectra (solid line) and PL spectra (dash line) of the product obtained with a molar ratio of $MnCl_2$ : $ZnAc_2$ at 0.25 : 1.

 

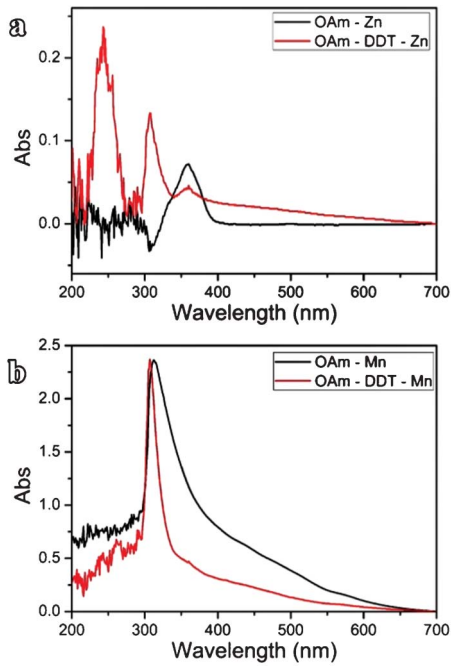


**Fig. 8** UV-vis absorption spectra of the solution obtained by dissolving different metal precursors in OAm (black line) or the mixture of OAm and DDT (red line). (a) $ZnAc_2{\cdot}2H_2O$, (b) $MnCl_2$.

1-dodecanethiol play an important role in the formation of the ED-NCs.

## Conclusions

In summary, the elongated Mn-doped $ZnSe_{1-x}S_x$ nanocrystals in the cubic phase have been synthesized through a facile one-pot method without complicated preparation before the synthesis. The ED-NCs show an average diameter of about 2–4 nm and length up to 10 nm. The small dimension of these nanocrystals enables them to display an obvious quantum-size effect, which has been confirmed by UV-vis absorption spectra. The successful doping of $Mn^{2+}$ into the ED-NCs is supported by the hyperfine splitting constant from EPR spectra and the emission band from PL spectra. The additional growth of a shell on the ED-NCs enhances the quantum yield of the emission from 20% up to 35%, which might benefit the applications of the doped nanocrystals in optoelectronics, biological imaging and ultrasensitive detection. The ED-NCs are probably produced *via* the growth-doping strategy, because the formation of the $ZnSe_{1-x}S_x$ nanocrystals is prior to the Mn doping based on UV-vis absorption spectra and PL spectra. It is believed that this method could be extended to the doping of other transition metal ions into anisotropic semiconductor nanoparticles.

## Acknowledgements

This work was supported by Natural Science Foundation of China (No. 21071055, 51172076), New Century Excellent Talents in University (NCET-10-0369), Guangdong Provincial Natural Science Foundation of China, New Faculty Start-up funding in Shandong University and Independent Innovation Foundations of Shandong University (2012ZD007), Shandong Provincial Natural Science Foundation for Distinguished Young Scholar. The authors thank Prof. Bin Zhang in Shandong University for PL measurements, Prof. Qing Yang in University of Science and Technology of China for EPR spectra and Prof. Narayan Pradhan in Indian Association for the Cultivation of Science for helpful discussion.

## References

1 J. H. Yu, X. Y. Liu, K. E. Kweon, J. Joo, J. Park, K. T. Ko, D. W. Lee, S. P. Shen, K. Tivakornsasithorn and T. Hyeon, *et al.*, *Nat. Mater.*, 2010, **9**, 47–53.
2 N. Pradhan, D. M. Battaglia, Y. C. Liu and X. G. Peng, *Nano Lett.*, 2007, **7**, 312–317.
3 P. T. Shao, H. Z. Wang, Q. H. Zhang and Y. Li, *J. Mater. Chem.*, 2011, **21**, 17972.
4 P. K. Santra and P. V. Kamat, *J. Am. Chem. Soc.*, 2012, **134**, 2508–2511.
5 M. Kaczmarek and M. Bredol, *J. Mater. Sci.*, 2011, **46**, 5400–5405.
6 D. J. Norris, N. Yao, F. T. Charnock and T. A. Kennedy, *Nano Lett.*, 2001, **1**, 3–7.
7 L. J. Zu, A. W. Wills, T. A. Kennedy, E. R. Glaser and D. J. Norris, *J. Phys. Chem. C*, 2010, **114**, 21969–21975.
8 N. S. Karan, D. D. Sarma, R. M. Kadam and N. Pradhan, *J. Phys. Chem. Lett.*, 2010, **1**, 2863–2866.
9 R. S. Zeng, T. T. Zhang, G. Z. Dai and B. Zou, *J. Phys. Chem. C*, 2011, **115**, 3005–3010.
10 J. Y. Lee, D. S. Kim, J. H. Kang, S. W. Yoon, H. Lee and J. Park, *J. Phys. Chem. B*, 2006, **110**, 25869–25874.
11 S. Bhattacharyya, I. Perelshtein, O. Moshe, D. H. Rich and A. Gedanken, *Adv. Funct. Mater.*, 2008, **18**, 1641–1653.
12 P. T. K. Chin, J. W. Stouwdam and R. A. Janssen, *Nano Lett.*, 2009, **9**, 745–750.
13 M. Zhang, Y. Lu, J. F. Chen, T. K. Zhang, Y. Y. Liu, Y. Yang, W. T. Yao and S. H. Yu, *Langmuir*, 2010, **26**, 12882–12889.
14 Z. T. Deng, L. Tong, M. Flores, S. Lin, J. X. Cheng, H. Yan and Y. Liu, *J. Am. Chem. Soc.*, 2011, **133**, 5389–5396.
15 V. L. Vegard, *Z. Phys.*, 1921, **5**, 17–26.
16 R. Viswanatha, D. M. Battaglia, M. E. Curtis, T. D. Mishima, M. B. Johnson and X. G. Peng, *Nano Res.*, 2008, **1**, 138–144.
17 Y. A. Wu and J. H. Warner, *J. Mater. Chem.*, 2012, **22**, 417–424.
18 R. Sathiyanarayanan, M. Alimohammadi, Y. Zhou and K. A. Fichthorn, *J. Phys. Chem. C*, 2011, **115**, 18983–18990.
19 R. L. Penn and J. F. Banfield, *Science*, 1998, **281**, 969–971.
20 N. Pradhan, H. F. Xu and X. G. Peng, *Nano Lett.*, 2006, **6**, 720–724.
21 Z. G. Li, J. H. Sui, X. L. Li and W. Cai, *Langmuir*, 2011, **27**, 2258–2264.
22 P. D. Cozzoli, L. Manna, M. L. Curri, S. Kudera, C. Giannini, M. Striccoli and A. Agostiano, *Chem. Mater.*, 2005, **17**, 1296–1306.
23 J. Yang, C. Xue, S. H. Yu, J. H. Zeng and Y. T. Qian, *Angew. Chem., Int. Ed.*, 2002, **41**, 4697–4700.
24 T. T. Yao, Q. Zhao, Z. P. Qiao, F. Peng, H. J. Wang, H. Yu, C. Chi and J. Yang, *Chem.–Eur. J.*, 2011, **17**, 8663–8670.
25 N. Pradhan, D. Goorskey, J. Thessing and X. G. Peng, *J. Am. Chem. Soc.*, 2005, **127**, 17586–17587.
26 R. Parrot, C. Naud, F. Gendron, C. Porte and M. Lemercier, *J. Chem. Phys.*, 1986, **85**, 4932–4937.
27 B. B. Srivastava, S. Jana, N. S. Karan, S. Paria, N. R. Jana, D. D. Sarma and N. Pradhan, *J. Phys. Chem. Lett.*, 2010, **1**, 1454–1458.
28 S. Acharya, D. D. Sarma, N. R. Jana and N. Pradhan, *J. Phys. Chem. Lett.*, 2010, **1**, 485–488.
29 C. Wang, X. Gao, Q. Ma and X. Su, *J. Mater. Chem.*, 2009, **19**, 7016–7022.
30 N. Dixit, H. Soni, M. Chawda and D. Bodas, *Mater. Lett.*, 2009, **63**, 2669–2671.
31 Y. G. Yang, O. Chen, A. Angerhofer and Y. C. Cao, *J. Am. Chem. Soc.*, 2006, **128**, 12428–12429.
32 N. Pradhan and X. G. Peng, *J. Am. Chem. Soc.*, 2007, **129**, 3339–3347.
33 X. H. Zhong, Y. Y. Feng and Y. Zhang, *J. Phys. Chem. C*, 2007, **111**, 526–531.
34 Z. H. Zhang, M. H. Lu, H. R. Xu and W. S. Chin, *Chem.–Eur. J.*, 2007, **13**, 632–638.